Lawrence Berkeley National Laboratory
Recent Work

Title
Defect Equilibration and Intrinsic Stress in Undoped Hydrogenated Amorphous Silicon

Permalink
https://escholarship.org/uc/item/4823d6tm

Authors
Kitsuno, Y.
Cho, G.
Drewery, J.
et al.

Publication Date
1993-07-01

eScholarship.org Powered by the California Digital Library
University of California

LBL-34360
UC-414
Preprint

Lawrence Berkeley Laboratory
UNIVERSITY OF CALIFORNIA

Physics Division

Submitted to Japanese Journal of Applied Physics

Defect Equilibration and Intrinsic Stress in Undoped Hydrogenated Amorphous Silicon

Y. Kitsuno, G. Cho, J. Drewery, W.S. Hong,
and V. Perez-Mendez

July 1993

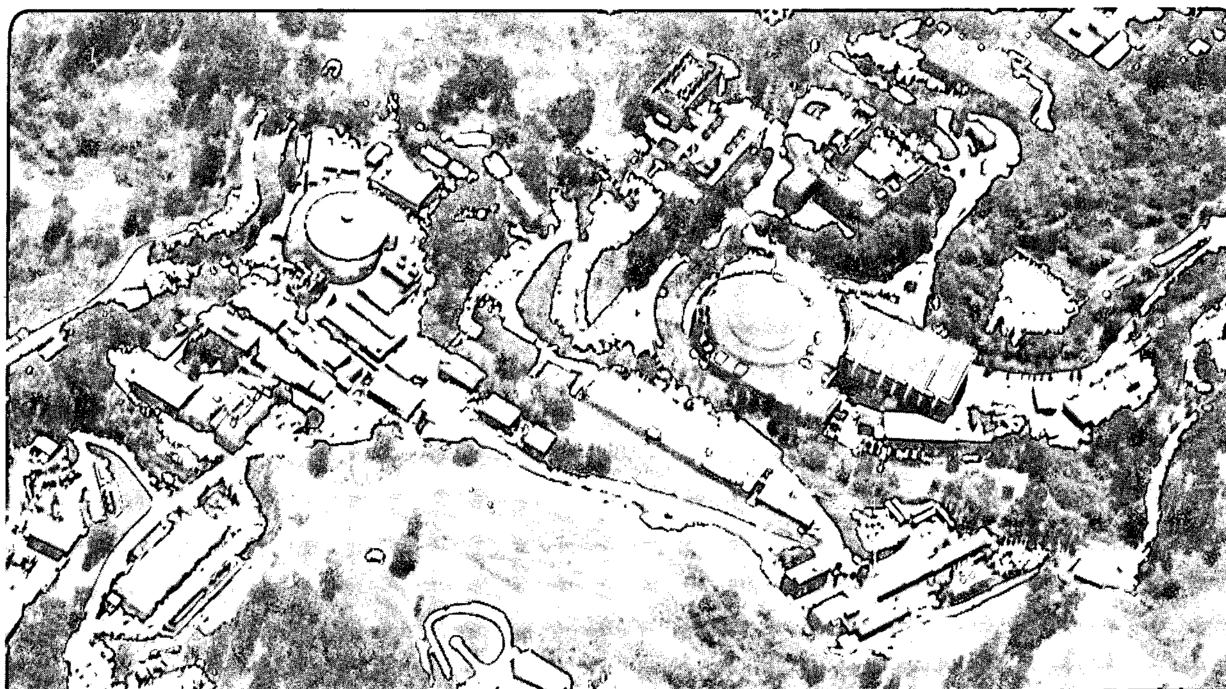

REFERENCE COPY
Does Not
Circulate
Bldg. 50 Library.
LBL-34360
Copy 1

Prepared for the U.S. Department of Energy under Contract Number DE-AC03-76SF00098

DISCLAIMER

This document was prepared as an account of work sponsored by the United States Government. While this document is believed to contain correct information, neither the United States Government nor any agency thereof, nor the Regents of the University of California, nor any of their employees, makes any warranty, express or implied, or assumes any legal responsibility for the accuracy, completeness, or usefulness of any information, apparatus, product, or process disclosed, or represents that its use would not infringe privately owned rights. Reference herein to any specific commercial product, process, or service by its trade name, trademark, manufacturer, or otherwise, does not necessarily constitute or imply its endorsement, recommendation, or favoring by the United States Government or any agency thereof, or the Regents of the University of California. The views and opinions of authors expressed herein do not necessarily state or reflect those of the United States Government or any agency thereof or the Regents of the University of California.

LBL-34360
UC-414

Defect Equilibration and Intrinsic Stress in Undoped Hydrogenated Amorphous Silicon

Y. Kitsuno,* G. Cho, J. Drewery, W. S. Hong, V. Perez-Mendez

Physics Division
Lawrence Berkeley Laboratory
University of California
Berkeley, California 94720

* On leave from, Showa Denko K.K., Chemicals Research Laboratory, 5-1 Ohgi-machi, Kawasaki-ku, Kawasaki, 210, Japan

July 1993

This work was supported by the Director, Office of Energy Research, Office of High Energy and Nuclear Physics, Division of High Energy Physics, of the U.S. Department of Energy under Contract No. DE-AC03-76SF00098.

Defect Equilibration and Intrinsic Stress in Undoped Hydrogenated Amorphous Silicon

Yu KITSUNO,* Gyuseong CHO, John DREWERY, Wan-Shick HONG and Victor PEREZ-MENDEZ

Lawrence Berkeley Laboratory, 1 Cyclotron Road, Berkeley, California 94720, U.S.A.

* On leave from, Showa Denko K.K., Chemicals Research Laboratory, 5-1 Ohgi-machi, Kawasaki-ku, Kawasaki, 210, Japan

KEYWORDS: **amorphous silicon, thermal equilibrium, ESR spin density, internal stress, time-of-flight (TOF), mobility-lifetime product ($\mu\tau$), electron mobility (μ), metastable state**

ABSTRACT

Relaxation data for the thermal equilibrium defect densities in undoped a-Si:H are obtained by time-of-flight (TOF) measurement in the temperature range of 160° to 250°C. The internal stress in the material is also measured. The mobility-lifetime product of electrons ($\mu\tau$) increases from 0.5 x 10^{-7} to its equilibrium value of 2.2 x 10^{-7}

cm^2/V during the 160°C annealing. The equilibrium value of $\mu\tau$ is equivalent to the spin density (N_S) of about 1.1 x 10^{15} cm^{-3}. The N_S curves have a minimun value just before their equilibrium. The time dependence of the Ns relaxation follows a two-term stretched exponential form which corresponds to two metastable states, and each relaxation time is activated with activation energies of 1.10 to 1.20 eV. The thermal equilibrium N_S increases with temperature with an activation energy of 0.20 to 0.30 eV. The data for the second annealing at 160°C after the first long annealings at 200° and 250°C also follows the two-term stretched exponential form derived from the first annealing data. The result suggests the presence of a multivalley energy configuration at metastable states. The electron mobility (μ) increases slightly compared with the $\mu\tau$ changes, and no stress change is observed during the various annealing steps. It is concluded that the structural change is much smaller than the change in metastable-state densities during annealing in the temperature range of 160° to 250°C.

1. INTRODUCTION

Defect equilibration and metastability in undoped hydrogenated amorphous silicon (a-Si:H) have been studied by different kinds of measurements. The defect density in undoped a-Si:H has been found to reach a thermal equilibrium in the temperature range of 100° to 300°C. [1-7] Defect equilibration in undoped a-Si:H was first observed by Smith et al. by photothermal deflection spectroscopy (PDS) and constant-photocurrent measurements (CPM). [2] McMahon and Tsu found the thermal-equilibrium temperature T_E was 190° to 200°C in undoped a-Si:H. [3] Street and Winer investigated the frozen-in defects in a-Si:H with different deposition conditions by ESR measurements in the temperature range of 180° to 400°C, and used a stretched exponential form for describing annealing bahavior. [4] Xu et al. observed temperature dependence of the thermal-equilibrium defect density in undoped a-Si:H and a-Si-based alloys by ESR measurements. [5-7] In these studies, the thermal-equilibrium defect density increases with temperature, and the high-temperature state above T_E can be frozen-in by quenching to room temperature, where the relaxation time is extremely long. McMahon found the time constants for annealings of 250°C fast-cool (FC) defects in a high-frequency film deposited by rf glow discharge at 110 MHz to be

activated with a barrier of 2.20 eV, and equilibrium spin densities also to be activated with a formation energy of 0.35 eV. [8] The activation energy of 0.35 eV is in good agreement with the value of about 0.3 eV in earlier studies. [9,10] The energy barrier of 2.20 eV is larger than the 1.50 eV measured on a sample made at high rf power. [4] Based on the crossover in one annealing data curve, McMahon suggested a multivalley energy configuration coordinate diagram with smaller barriers between metastable states to describe defect states in a-Si:H films. [11]

Generally a-Si:H films have large amounts of intrinsic stress. [12-16] Previous studies have shown that the amount of stress depends on the silane concentration used for film growth, [12] the deposition temperature, [13] the rf power, [13,14] and the ratio of dihydride (SiH_2) to monohydride (SiH) content in the films. [14] Stevens and Johnson showed that the maximum compressive stress appeared under the same conditions in which the optimized electronic properties were obtained. [15] Kurtz et al. found no correlation between stress and the light-induced effect which causes metastable defects. [16]

Basic material parameters in a-Si:H: electron mobility (μ) and mobility-lifetime product of electrons ($\mu\tau$) were obtained by TOF measurement using a pulsed laser system. [17]

In this work, we study both the relaxation behavior of frozen-in defects in undoped a-Si:H and the temperature dependence of the thermal-equilibrium defect density by using TOF measurements, as

well as the energy configuration at matastable states using relaxation data of the various pre-annealing conditions. We use a two-term exponential form instead of the single-term form used in earlier studies for describing the time dependence of the Ns relaxation. [4,7,8,11] We also measure the internal stress in a-Si:H during the various annealing steps to describe relationship between the behavior of metastability and the structural changes of a-Si:H.

2. EXPERIMENTAL

The a-Si:H samples used in this study were prepared by rf glow discharge from SiH_4. The rf power was 7 W at 85 MHz. Films of 14 μm thickness were deposited on chromiun-coated Corning 7059 glass substrates held at 320°C. The samples had thin top (p^+) layers of p^+-a-Si_xC_{1-x}:H made from $SiH_4 + CH_4 + B_2H_6$ at 250°C. They had thin bottom (n^+) layers of n^+-a-Si:H made from $SiH_4 + PH_3$ at 320°C. Semi transparent chromium contacts were deposited on the p^+ layers of the films for making TOF measurements.

The samples were first annealed at 300°C for 10 minutes and then fast-cooled by dropping the samples into cool water. The samples were then annealed at temperatures of 160° to 250°C for increasing amounts of time. During the various annealing steps, the fast cools were performed in order to make TOF and internal stress measurements. After the $\mu\tau$ of the samples reached an equilibrium at

200° or 250°C, additional 160°C annealings were performed for further measurements.

The transient photoconductivity of a-Si:H was measured to obtain μ and $\mu\tau$ using a 510-nm pulsed laser system with 3-ns pulse width. The 510-nm light has a mean free path of about 0.2 μm and can be used to provide information about the electron signal when the light is incident on the p^+ layer of the sample. The mobility, μ, was obtained by measuring transient time signals in a conventional TOF experiment. The $\mu\tau$ product was obtained from the field dependence of collected charge and the Hecht equation.

The internal stress of a-Si:H was obtained by measuring the curvature of the underside of the glass substrates. [14] The curvature provides the following total stress;

$$\sigma_t = E_s t_s^2 / 6(1 - \nu_s) t_f R, \qquad (1)$$

where E_s is Young's modulus of the glass substrate, ν_s is Poisson's ratio of the substrate, t_s is the thicknesses of the substrate, t_f is the thickness of the a-Si:H film, and R is the radius of curvature of the deposited substrate. The total stress is a sum of the intrinsic stress (σ_i) and the differential thermal expansion between the film and the substrate;

$$\sigma_t = \sigma_i + (\alpha_s - \alpha_f)[E_f / (1 - \nu_f)](T_s - T_m), \qquad (2)$$

where α_s and α_f are the thermal expansion coefficients of the substrate and the a-Si:H film, E_f is Young's modulus of the a-Si:H, ν_f is Poisson's ratio of the a-Si:H, T_s is the deposition temperature, and T_m is the measurement temperature. The values used for the calculations were $E_s = 6.8 \times 10^{10}$ Pa, $\nu_s = 0.28$, $E_f = 4.4 \times 10^{10}$ Pa, $\nu_f = 0.2$, $\alpha_s = 4.6 \times 10^{-6}°C^{-1}$, $\alpha_f = 4 \times 10^{-6}°C^{-1}$, $T_s = 320°C$, and $T_m = 25°C$. [16]

3. RESULTS AND DISCUSSION

3.1 *Defects*

The time dependence of $\mu\tau$ for different annealing temperatures is shown in Fig. 1. The $\mu\tau$ changes from its initial value of 0.5×10^{-7} to an equilibrium value of 2.2×10^{-7} cm^2V^{-1} at 160°C. The initial value in each series of measurements was the same within the experimental uncertainty. It takes about 2×10^6 sec at 160°C to reach equilibrium, and it decreases by two orders of magnitude at 250°C. It is noteworthy that a maximum value of $\mu\tau$ appears just before its equilibrium at each annealing temperature.

The spin density (N_S) was calculated from the value of $\mu\tau N_S = 2.5 \times 10^8$ $cm^{-1}V^{-1}$ [17]. The equilibrium value of $\mu\tau$ at 160°C is equivalent to a N_S of as low as 1.1×10^{15} cm^{-3}. The relaxation data for N_S are shown in Fig. 2. Like the $\mu\tau$ curves, all curves of N_S have a minimum value just before their equilibrium. For the purpose of

fitting the annealing data to the equation curve, earier studies have used the following stretched single-term exponential form;

$$N_S(t) = N_f + (N_i - N_f)\exp[-(t / t_R)^{\beta}], \qquad (3)$$

where N_i is the initial quenched-in spin density, N_f is the final annealing value, t_R is the relaxation time, and β is the dispersion parameter. [4,7,8,11] In this study the annealing data do not fit well to eq. (1) because of the minimum value before their equilibrium. In order to fit our experimental data, we adopted a new equation,

$$N_S(t) = N_1(t) + N_2(t), \qquad (4)$$

where $N_1(t)$ and $N_2(t)$ are the spin densities at the metastable state M_1 and M_2 shown in Fig. 3. There, S_0 indicates the stable state. Since $N_1(t)$ and $N_2(t)$ are time dependent,

$$dN_1(t) / dt = -t^{\beta_1 - 1} N_1(t), \qquad (5)$$

and

$$dN_2(t) / dt = -t^{\beta_2 - 1} N_2(t). \qquad (6)$$

They can be described by the stretched exponential forms,

$$N_1(t) = N_{f1} + (N_{i1} - N_{f1})\exp[-(t / t_{R1})^{\beta_1}], \qquad (7)$$

and

$$N_2(t) = N_{f2} + (N_{i2} - N_{f2})\exp[-(t / t_{R2})^{\beta_2}], \qquad (8)$$

where N_{i1} and N_{i2} are the initial quenched-in spin densities, N_{f1} and N_{f2} are the final annealing values, t_{R1} and t_{R2} are the relaxation times, and β_1 and β_2 are the dispersion parameters at M_1 and M_2. Here N_i and N_f are written as

$$N_i = N_{i1} + N_{i2}, \qquad (9)$$

and

$$N_f = N_{f1} + N_{f2}. \qquad (10)$$

In our experiments, since the first annealings for making quenched-in defects were performed for relatively short times, we can neglect N_{i2}.
Thus eq. (9) is replaced by

$$N_i = N_{i1}. \qquad (11)$$

Equation (4) becomes the following two-term exponential form,

$$N_S(t) = N_f + [N_i - (1 - x_T)N_f]\exp[-(t / t_{R1})^{\beta_1}] - x_T N_f \exp[-(t / t_{R2})^{\beta_2}], \quad (12)$$

with

$$N_{f1} = (1 - x_T)N_f, \quad (12a)$$

and

$$N_{f2} = x_T N_f, \quad (12b)$$

where x_T is a ratio of the final values and $0 < x_T < 1$. Then the annealing data for the a-Si:H samples fit well to eq. (12) curves shown in Fig. 2 with the fitting parameters listed in Table I.

As seen in Table I, the relaxation time t_{R1} of the quenched-in spin density at M_1 is 8×10^4 sec at 160°C, decreasing to 5.5×10^2 sec at 250°C. These values of t_{R1} are the same magnitude as the relaxation times reported by Xu et al [7]. In our study, the relaxation time t_{R2} at M_2 is an order of magnitude larger than t_{R1} at the same annealing temperature. It is assumed that the difference between t_{R1}

and t_{R2} is due to the differences in the initial spin densities at M_1 and M_2 and in the sites of M_1 and M_2.

The ratios of the final spin densities, x_T, range from 0.30 to 0.45. These values provide a distribution of equilibrium spin densities in the two-valley energy configuration of metastable states shown in Fig. 3.

The temperature dependence of N_f, N_{f1}, and N_{f2} is shown in Fig.4. N_{f1} and N_{f2} increase with temperature with activation energies of 0.27 eV and about 0.20 eV, shown respectively as ΔE_1 and ΔE_2 in Fig. 3. This fact suggests that the energy levels of the state M_1 and M_2 are probably almost the same within experimental uncertainty, providing the same order of final spin density in both metastable states. The value of 0.27 eV of ΔE_1 is nearly the same as about 0.30 eV or 0.35 eV in earlier studies. [9-11]

The temperature dependence of t_{R1} and t_{R2} is shown in Fig. 5. The relaxation times t_{R1} and t_{R2} are activated with energies of 1.10 eV and 1.15 eV, shown respectively as E_{B1} and E_{B2} in Fig. 3. The energy barrier of 1.10 eV is smaller than the 1.50 eV reported by Street and Winer [4] and the 2.20 eV reported by McMahon. [11] If the single-term exponential form were used to calculate our E_B, the E_B in this study would be about 1.30 eV, which is not so small when compared with the 1.50 eV, but which is considerably smaller than the 2.20 eV. This seems to be due to the differences in the film preparation method or in the cooling rate at which the quenched-in

defects were created. Although the values of t_{R1} and t_{R2} are an order of magnitude different at the same annealing temperatures, we obtained almost the same values for E_{B1} and E_{B2}. The presence of M_2 supports the multivalley energy configuration coordinate model proposed by McMahon. [11] In our study, however, the energy barrier between the two metastable states, M_1 and M_2, may be as high as that between S_0 and M_1 in Fig. 3. This configuration is different from McMahon's model, which shows smaller barriers between the metastable states.

In order to ascertain the presence of M_2, two second annealings at 160°C were performed after the first long annealings at 200°C and 250°C .

The time dependence of $\mu\tau$ during the second annealings is shown in Fig. 6. Achieving further equilibrium takes about 2 x 10^6 sec, which is almost the same as the time required for annealing at 160°C (the first annealing) in Fig. 1. The value of $\mu\tau$ changes from 1.0 x 10^{-7} to its equilibrium value of 1.4 x 10^{-7} cm^2/V at 160°C after the first 200°C annealing, and changes from 0.8 x 10^{-7} to its equilibrium value of 1.5 x 10^{-7} cm^2/V at 160°C after the first 250°C annealing. A maximum value of $\mu\tau$ appears just before its equilibrium during both 160°C annealings as well as during the first annealing.

The relaxation data for N_S during the second annealings are shown in Fig. 7. The equilibrium $\mu\tau$ values of 1.4 x 10^7 and 1.5 x 10^7 cm^2/V are equivalent to N_S of 1.8 x 10^{15} and 1.7 x 10^{15} cm^{-3},

respectively. In order to fit the second annealing data, we can rewrite eq. (4). Equation (4), with eqs. (7) - (10), becomes

$$N_S(t) = N_f + [(1 - x_{T1})N_i - (1 - x_{T2})N_f]\exp[-(t / t_{R1})^{\beta_1}] + (x_{T1}N_i - x_{T2}N_f)\exp[-(t / t_{R2})^{\beta_2}] \quad (13)$$

with

$$N_{i1} = (1 - x_{T1})N_i, \quad (13a)$$

$$N_{i2} = x_{T1}N_i, \quad (13b)$$

$$N_{f1} = (1 - x_{T2})N_f, \quad (13c)$$

and

$$N_{f2} = x_{T2}N_f, \quad (13d)$$

where x_{T1} and x_{T2} are the values of x_T at the temperatures of the first and the second annealing. The curve of N_S from eq. (13) is about the same as the experimental results shown in Fig. 7. This fact supports the presence of M_2, which corresponds to the two-term exponential form. If the single-term exponential form were used to calculate the relaxation time in our experiment, the values would be

7×10^5 sec for the second annealing after the long annealing at 200°C, 3×10^5 sec for the second annealing after the long annealing at 250°C, and 7×10^4 sec for the first annealing after the short annealing at 300°C. These data show that relaxation behavior depends strongly on the initial condition when annealing starts. Regardless of when the 160°C annealings are done in the sequence, the parameters for all 160°C annealings are the same except for the values of N_{i1}, N_{i2}, N_{f1}, and N_{f2} for the two exponential terms. The relaxation times t_{R1} and t_{R2}, and the dispersion parameters β_1 and β_2, are the same. Therefore it is assumed that the defect relaxation depends on the difference in the initial defect distributions in the metastable states.

The final N_S values, N_{f1} and N_{f2}, in the second annealing are a little lower than the N_S value of 1.1×10^{15} cm^{-3} for the first 160°C annealing. This fact indicates the presence of a third or several more metastable states, which are neglected in our calculation.

The defect mechanism suggested by Street and Winer is that hydrogen is released from a Si-H bond and breaks a weak Si-Si bond. At the Si-Si site, a new metastable state, M_1, and a new Si-H bond are created. [4)] In our study, we suggest that a mobile hydrogen, which has created a Si-H bond where a weak Si-Si bond used to be, is released again and breaks another weak bond, then a new metastable state is created at M_2 and a weak Si-Si bond is created again where M_1 used to be.

3.2 *Electron mobility*

The time dependence of μ for the first and second annealings are shown in Fig. 8(a) and 8(b), respectively. A small change correlated to the $\mu\tau$ is seen, and a maximum value of μ appear about the same time as that of $\mu\tau$. During the first 160°C annealing, μ changes from 1.07 to 1.23 cm^2/Vs at its equilibrium. Generally the carrier mobility is reduced by scattering, which increases with the degree of disorder, and the energy of the mobility edge within the band also depends on the degree of disorder. [18] When metastable defects are introduced by quenching-in at the initial FC, the degree of disorder in the a-Si:H rises and the mobility edge within the band becomes less steep. As metastable defects decrease during annealing, the degree of disorder decreases and the mobility edge becomes steeper. Since the relative change of μ is smaller than that of $\mu\tau$, the relative change of the degree of disorder is also smaller than that of N_S. The degree of disorder, which will be discussed in the next section, should correspond with the Si-Si network and the Si-H bond structure.

3.3 *Internal stress*

The time dependence of normalized internal stress is shown in Fig. 9. The initial values of internal stress in samples we measured were between 260 and 350 MPa. In Fig. 9, no change in internal

stress was observed within the experimental uncertainty. The origin of stress, as well as the degree of disorder, should be due to the Si-Si network and Si-H bond structure. Though mobile hydrogen can change the network and the bond structure by breaking weak bonds, the number of broken bonds will be much smaller than the number of total Si-Si bonds in the a-Si:H. The number of broken weak bonds (N_{BW}) at the initial annealing stage will be written as

$$N_{BW} = (N_i - N_f) / 2. \quad (14)$$

In this study, N_{BW} is 2×10^{15} cm^{-3} for a 160°C annealing. This value is between 2×10^{-8} and 3×10^{-8} times as low as the total number of Si-Si bonds. Therefore it is assumed that metastable-state density changes, which are caused by mobile hydrogen, are not enough to cause the structural change which affects the observable change in the stress at temperatures between 160° and 250°C, temperatures which will not cause irreversible change in the film properties. Though the structural change is too small to change the stress, the degree of disorder is changed slightly, resulting in a relatively small change of μ. It is concluded that the change in metastable-state densities may affect some kinds of film properties along the following lines: $\mu\tau$ and N_S change by factors of 5; μ changes by 15 %; and changes in stress are not observable.

4. CONCLUSIONS

TOF measurements provide relaxation data for mobility-lifetime products ($\mu\tau$) and mobilities (μ) of electrons in undoped a-Si:H. Thermal equilibration spin density (N_S) derived from $\mu\tau$ is observed between 160° and 250°C. The N_S curves have a minimum value just before their equilibrium. The time dependence of the Ns relaxation follows a two-term stretched exponential form which corresponds to two metastable states, and each relaxation time is activated with activation energies of 1.10 to 1.20 eV. The thermal equilibrium N_S increases with temperature with an activation energy of 0.20 to 0.30 eV. Relaxation data, including the data for the second annealings, confirm the presence of a multivalley energy configuration at the metastable states.

Compared with the $\mu\tau$ change, there is a slight increase in μ, and no stress change is observed during the various annealing steps. We conclude that the change in metastable-state densities affect some kinds of film properties: $\mu\tau$ and N_S change by factors of 5; μ changes by 15 %; and changes in stress are not observable.

ACKNOWLEDGEMENTS

This study was supported by the U.S. Department of Energy under Contact No. DE-AC03-76SF00098.

One of us Yu Kitsuno would like to thank the management of Showa Denko K.K. for supporting his stay in Berkeley.

<References>

1) Z. E. Smith and S. Wagner: Phys. Rev. **B32** (1985) 5510.

2) Z. E. Smith, S. Aljishi, D. Slobodin, V. Chu, S. Wagner, P. M. Lenahan, R. R. Arya and M. S. Bennett: Phys. Rev. Lett. **57** (1986) 2450.

3) T. J. McMahon and R. Tsu: Appl. Phys. Lett. **51** (1987) 412.

4) R. A. Street and K. Winer: Phys. Rev. **B40** (1989) 6236.

5) X. Xu, A. Morimoto, M. Kumeda and T. Shimizu: Appl. Phys. Lett. **52** (1988) 622.

6) X. Xu, A. Okumura, A. Morimoto, M. Kumeda and T. Shimizu: Phys. Rev. **B38** (1988) 8371.

7) X. Xu, H. Sasaki, A. Morimoto, M. Kumeda and T. Shimizu: Phys. Rev. **B41** (1990) 10049.

8) T. J. McMahon: Solar Cells **30** (1991) 235.

9) J. Kakalios and W. B. Jackson: *Amorphous Silicon and Related Materials*, ed. H. Fritzsche (World Scientific, Singapore, 1988), p. 209.

10) S. Zafer and E. A. Schiff: J. Non-Cryst. Solids **114** (1989) 618.

11) T. J. McMahon: Phys. Rev. **B45** (1992) 4512.

12) J. P. Habison, A. J. Williams and D. V. Lang: J. Appl. Phys. **55** (1984) 946.

13) K. Ozawa, N. Takagi and K. Asama: Jpn. J. Appl. Phys. **22** (1983) L801.

14) H. Kakinuma, S. Nishikawa, T. Watanabe and K. Nihei: J. Appl. Phys **59** (1986) 3110.

15) K. S. Stevens and N. M. Johnson: J. Appl. Phys. **71** (1992) 2628.

16) S. R. Kurtz, Y. S. Tsuo and R. Tsu: Appl. Phys. Lett. **49** (1986) 951.

17) S. Qureshi, V. Perez-Mendez, S. N. Kaplan, I. Fujieda, G. Cho and R. A. Street: J. Non-Cryst. Solids **114** (1989) 417.

18) R. A. Street: *Hydrogenated amorphous silicon*, eds. R. W. Cahn, E. A. Davis and I. M. Ward (Cambridge University Press, Cambridge, 1991), p. 14-15.

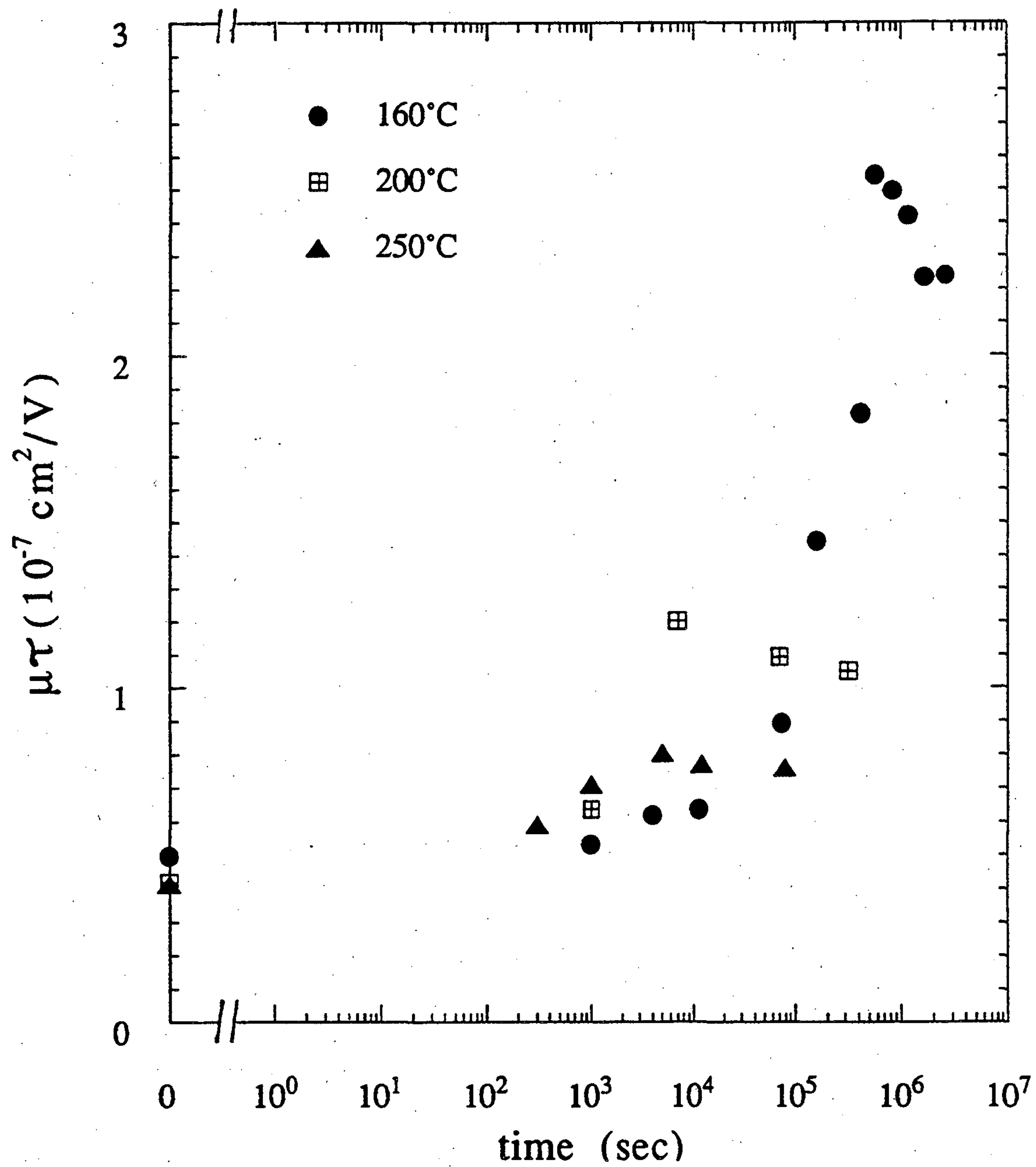

Fig. 1. Time dependence of $\mu\tau$ during annealings at different temperatures after quenching from 300°C.

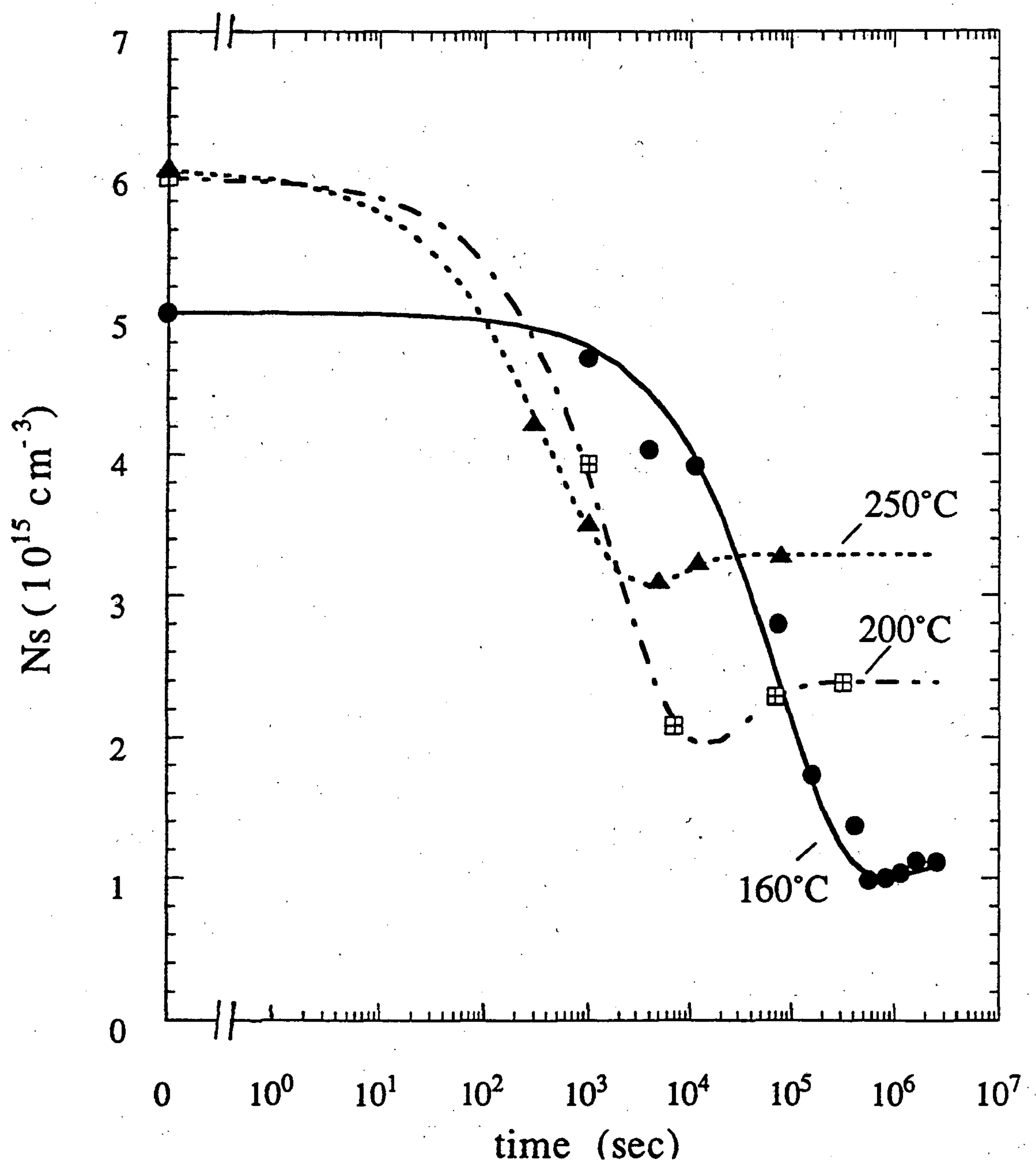

Fig. 2. Relaxation data for the spin densities at different temperatures after quenching from 300°C. The curves are the results fitted with eq. (12).

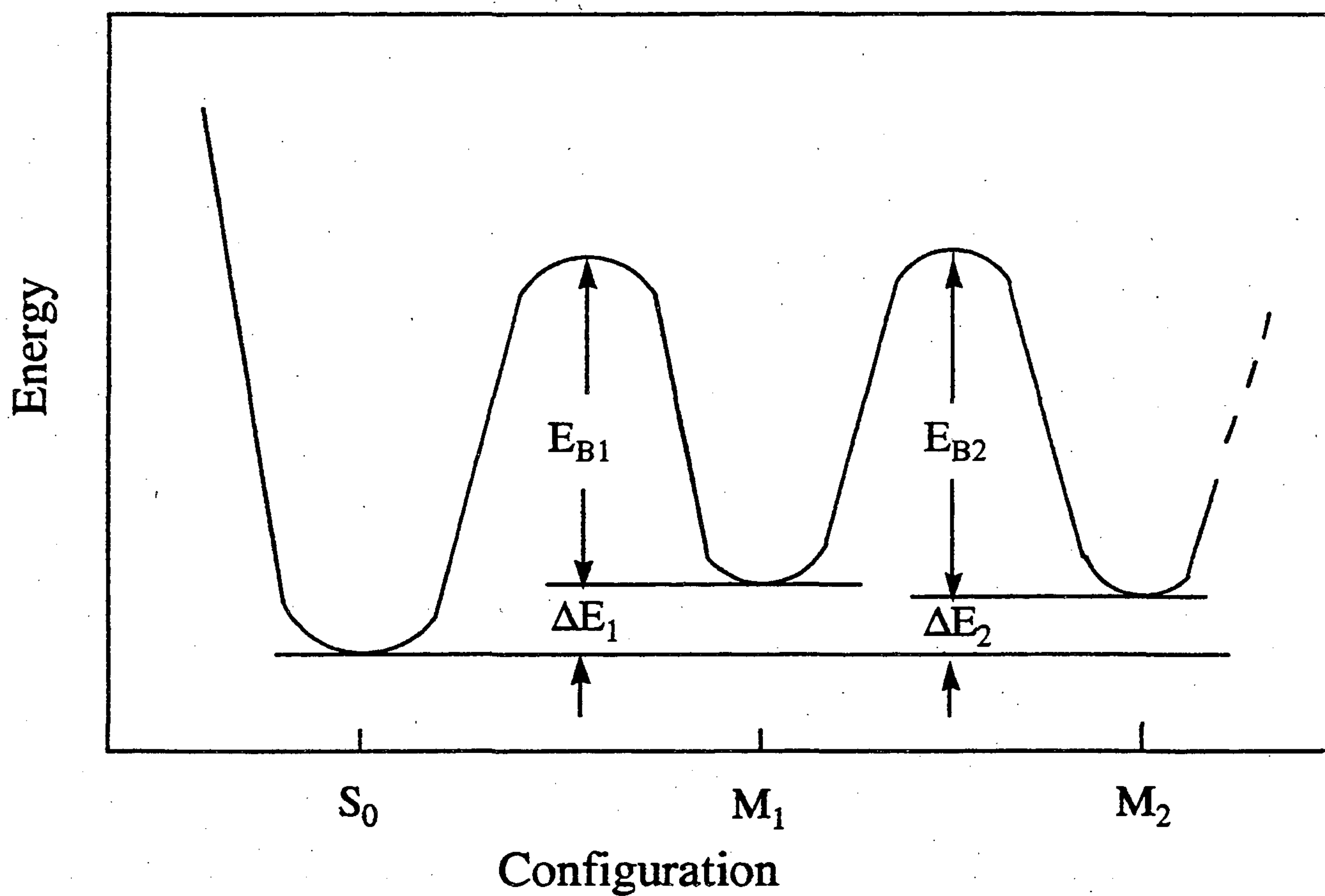

Fig. 3. Multivalley energy configuration graph, showing the metastable states (M_1 and M_2) and the stable state (S_0). The figure is explained in the text.

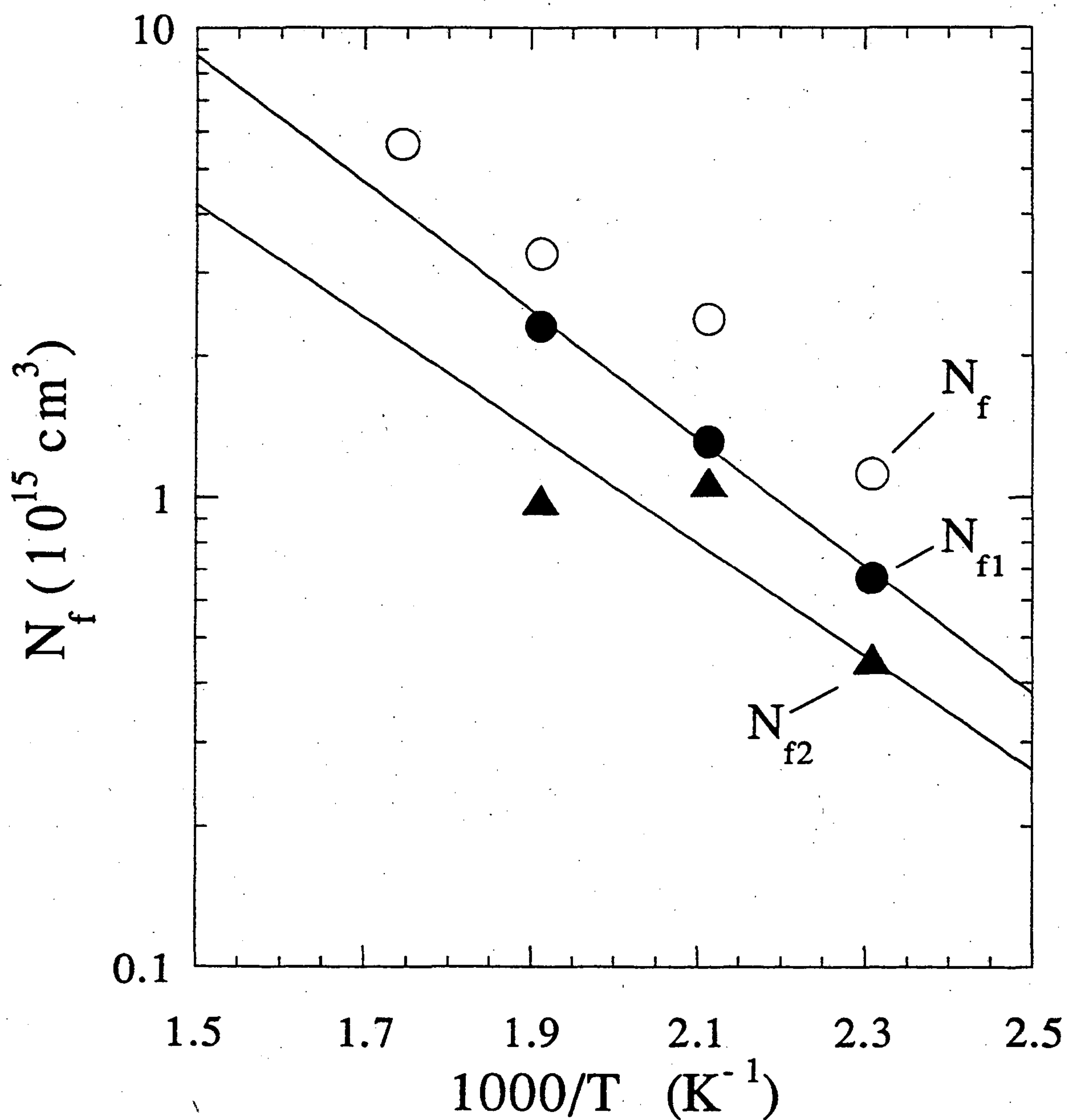

Fig. 4. Temperature dependence of final values of spin density. N_f is the total value, and N_{f1} and N_{f2} are the values at metastable states M_1 and M_2.

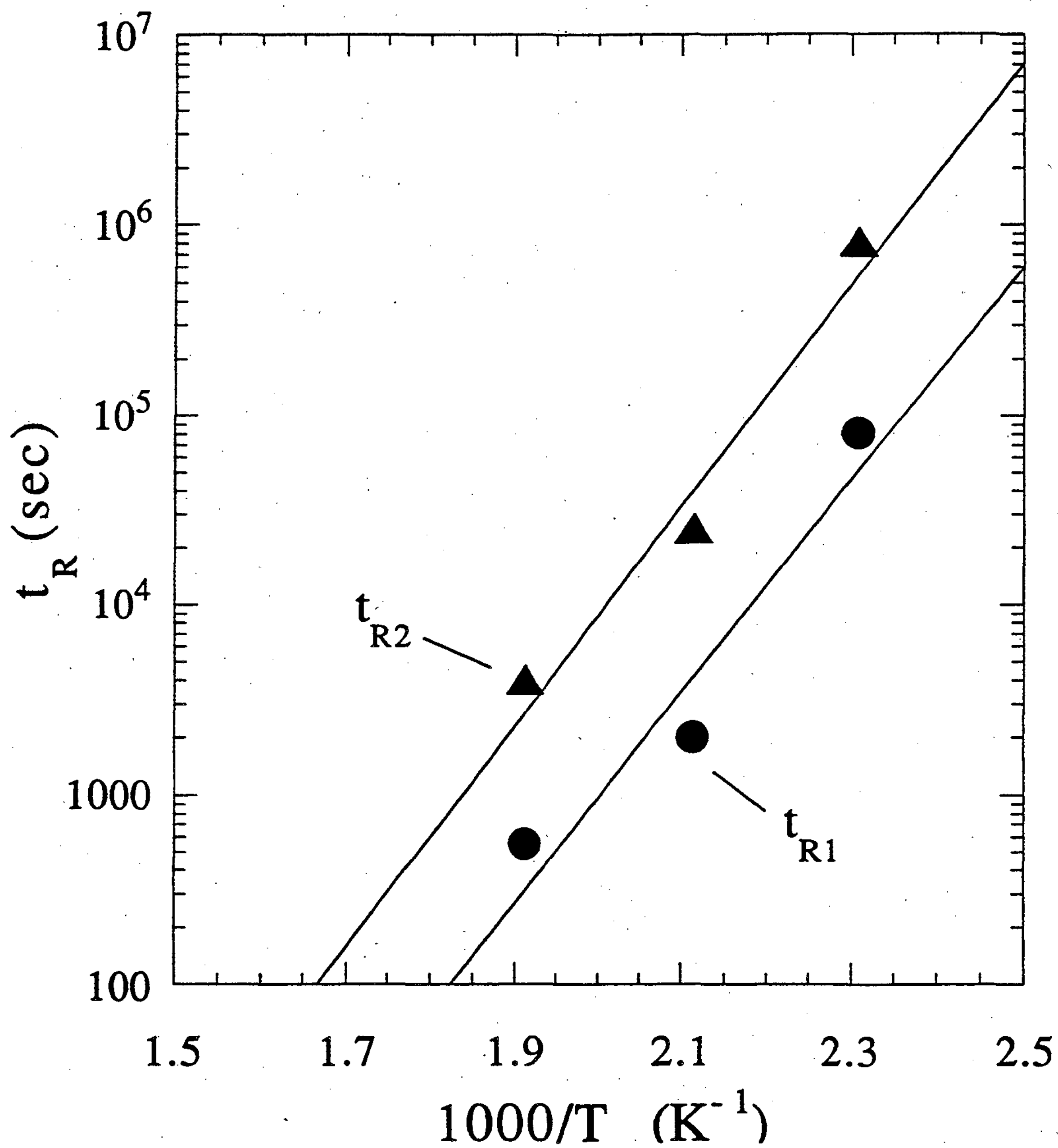

Fig. 5. Temperature dependence of relaxation times. Times t_{R1} and t_{R2} are the values at metastable states M_1 and M_2.

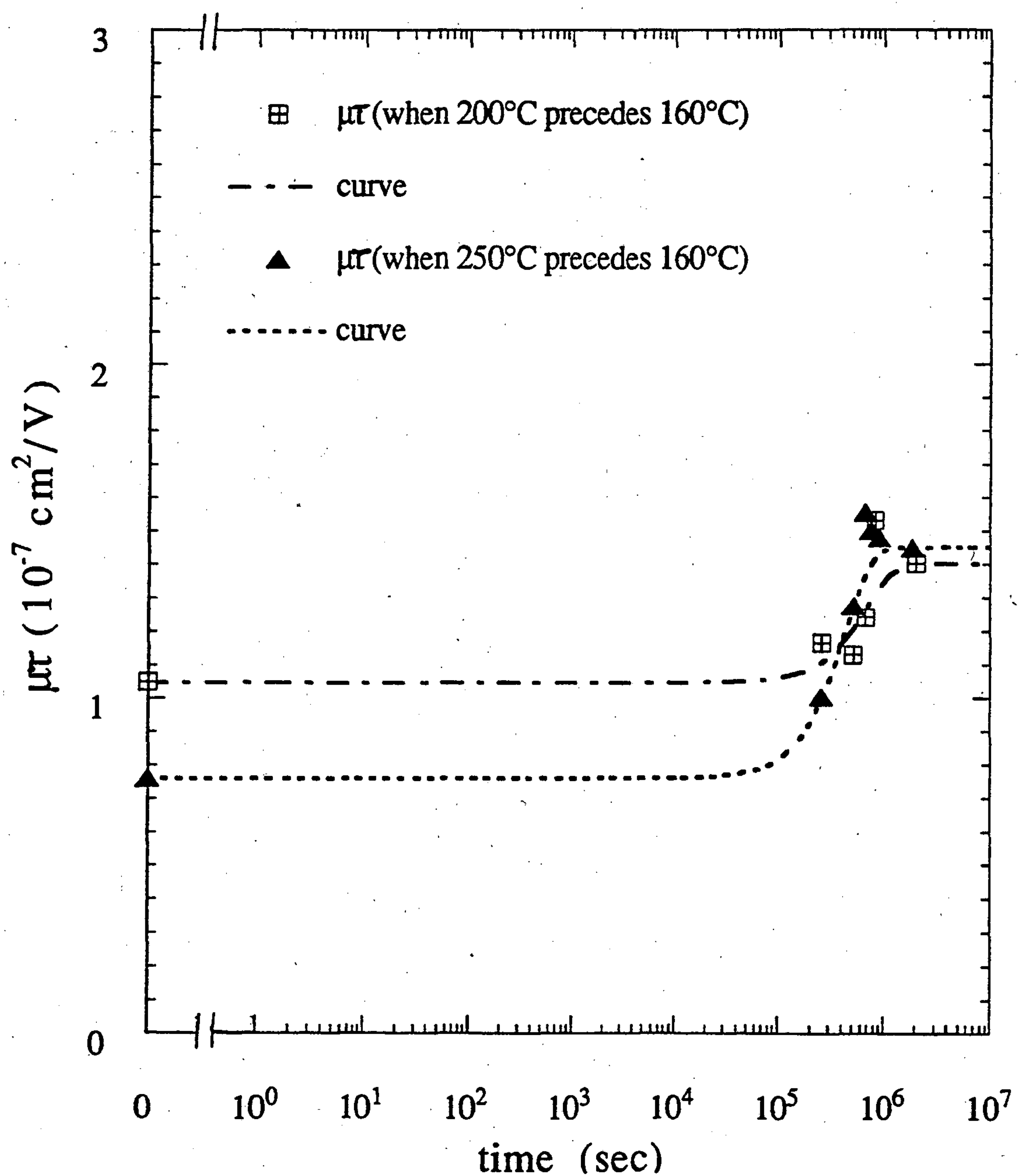

Fig. 6. Time dependence of μτ during the second annealings at 160°C. The 160°C annealing following the 200°C annealing is shown by squares, and the 160°C annealing following the 250°C annealing is shown by triangles. The curves are guides for the eye.

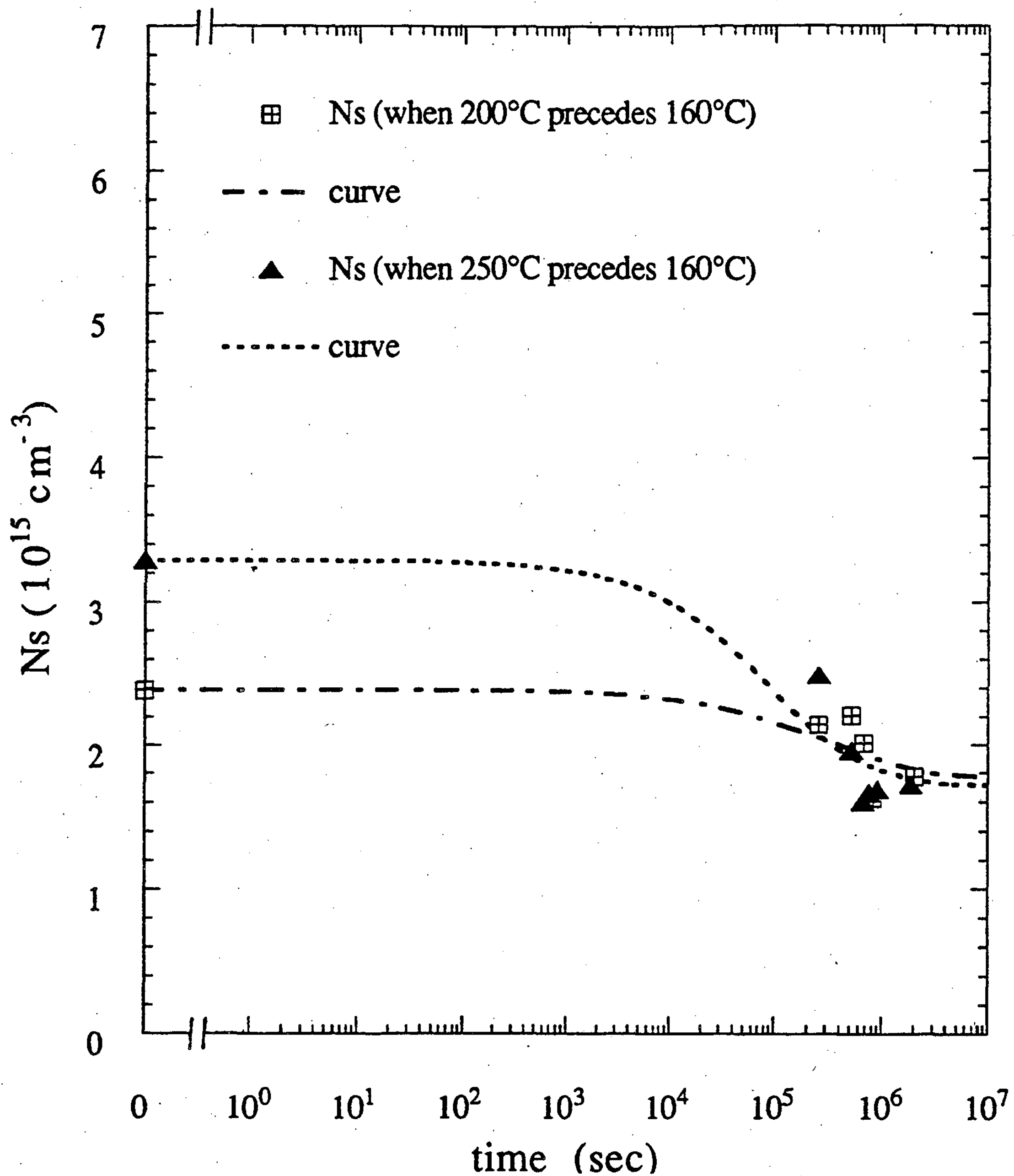

Fig. 7. Relaxation data for the spin densities at 160°C. Spin density during the 160°C annealing following the 200°C annealing is shown by squares, and spin density during the 160°C annealing following the 250°C annealing is shown by triangles. The curves are the results fitted with eq. (13).

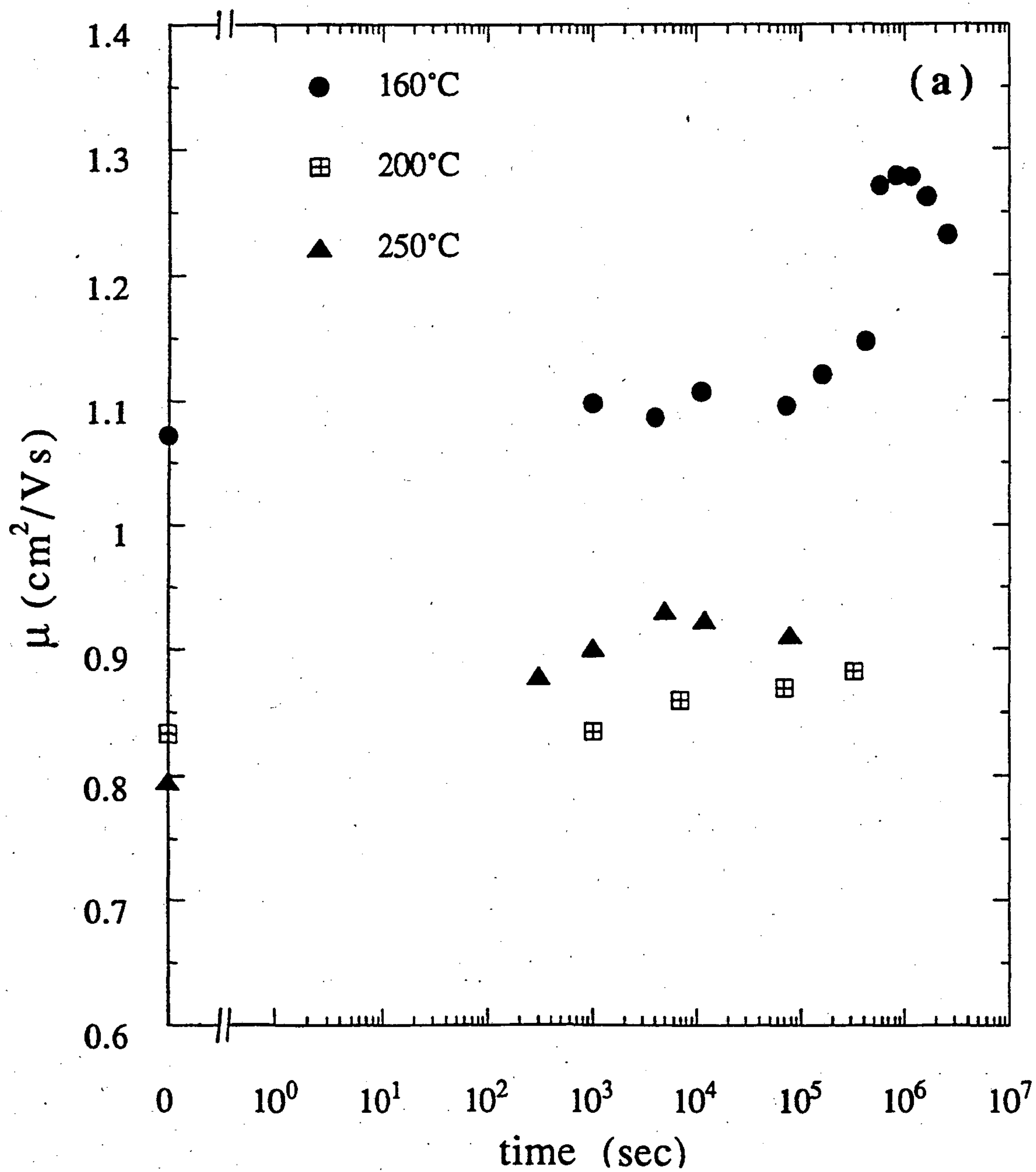

Fig. 8(a). Time dependence of μ during annealings at different temperatures after quenching from 300°C.

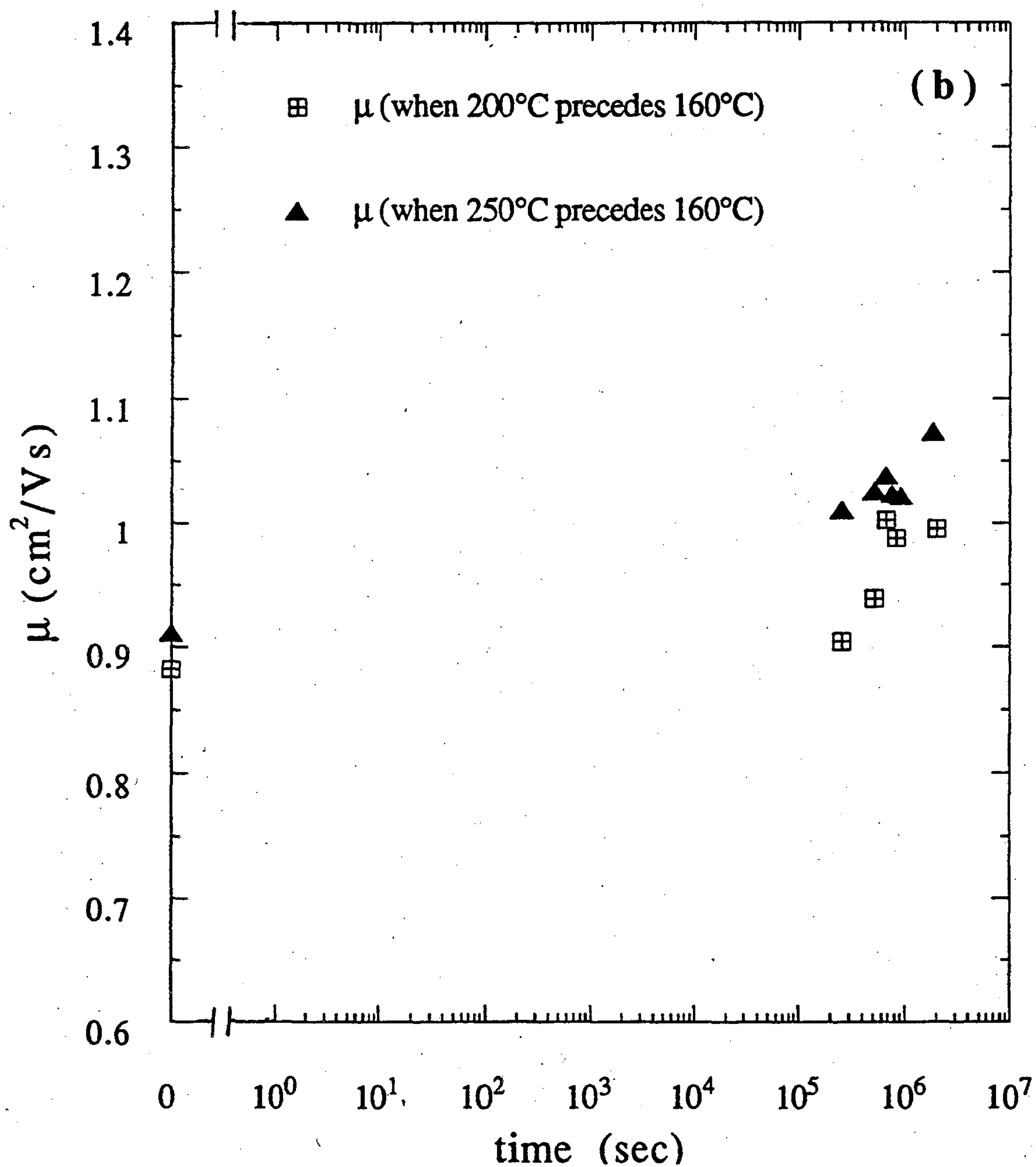

Fig. 8(b). Time dependence of μ during the second annealings at 160°C. The 160°C annealing following the 200°C annealing is shown by squares, and the 160°C annealing following the 250°C annealing is shown by triangles.

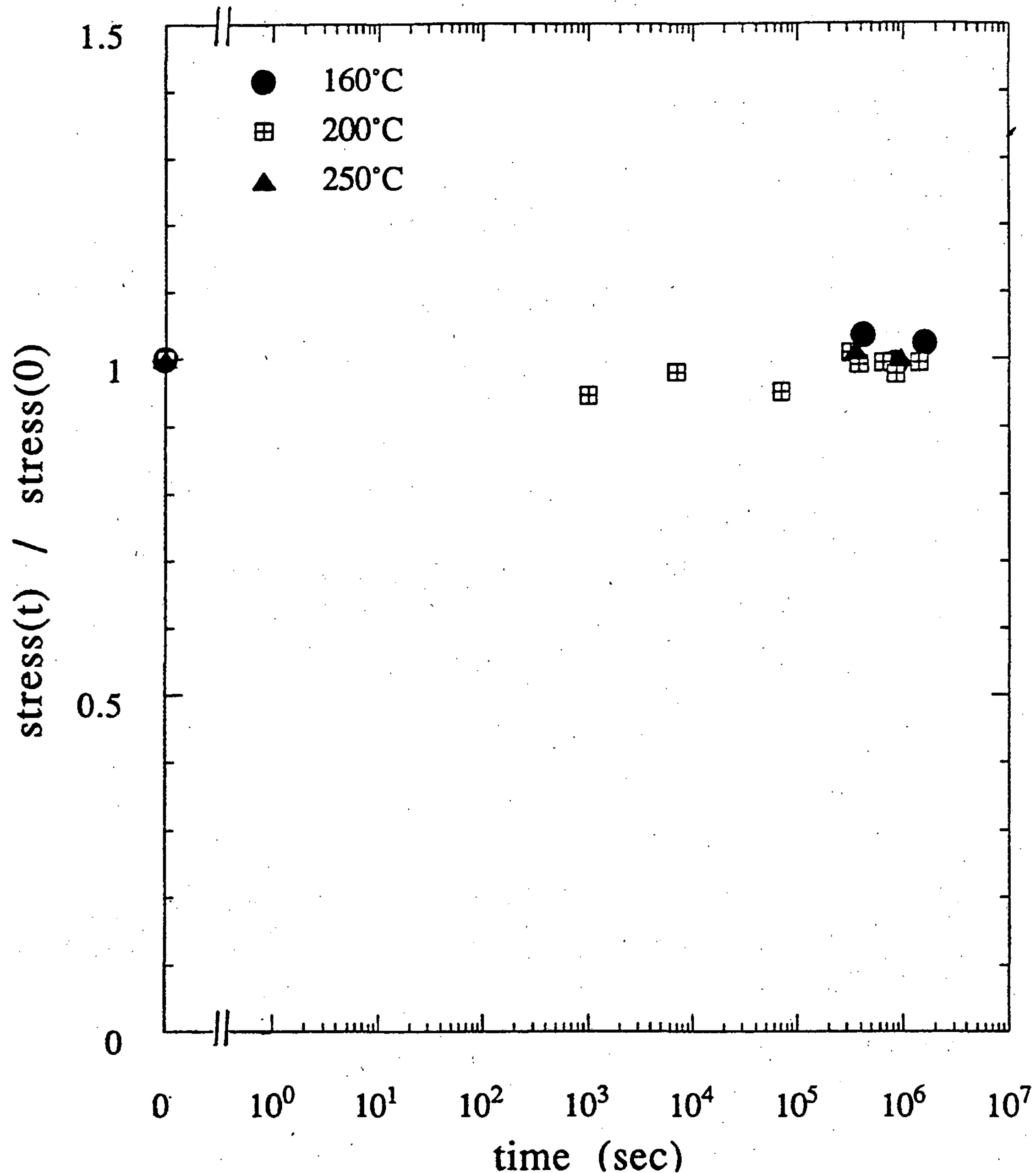

Fig. 9. Time dependence of normalized internal stress during annealings at different temperatures. After the 160°C annealings begin, the data from those annealings as well as from the earlier 200°C and 250°C annealing are included. The time dependence during the 200°C annealing and the 160°C annealing following it is shown by squares. The time dependence during the 250°C annealing and the 160°C annealing following it is shown by triangles.

Table I. Fitting parameters used with Eq. (12) for the curves shown in Fig. 2

annealing temperature	160°C	200°C	250°C
N_i (10^{15} cm^{-3})	5.02	5.97	6.04
N_f (10^{15} cm^{-3})	1.12	2.39	3.29
x_T	0.40	0.45	0.30
t_{R1} (sec)	8×10^4	2×10^3	5.5×10^2
t_{R2} (sec)	8×10^5	2.5×10^4	4×10^3
β_1	0.65	0.65	0.60
β_2	0.80	0.80	0.80

LAWRENCE BERKELEY LABORATORY
UNIVERSITY OF CALIFORNIA
TECHNICAL INFORMATION DEPARTMENT
BERKELEY, CALIFORNIA 94720